JOURNAL OF COMPUTATIONAL PHYSICS **44**, 46–69 (1981)

3D Nonlinear Calculations of Resistive Tearing Modes*,†

H. R. HICKS, B. CARRERAS, J. A. HOLMES, D. K. LEE, AND B. V. WADDELL‡

Oak Ridge National Laboratory, Oak Ridge, Tennessee 37830

Received November 12, 1980; revised May 5, 1981

Recent numerical calculations of the evolution of resistive tearing modes have been central to the understanding of MHD activity and disruptions in tokamaks. The nonlinear three-dimensional initial value computer code *RSF* has provided many of these results. *RSF* assumes cylindrical geometry with a Fourier series representation in the two periodic coordinates and a finite difference representation in the radial direction. This choice makes *RSF* considerably more accurate and efficient than previous codes.

1. INTRODUCTION

The tokamak has emerged as one of the most promising magnetic confinement devices for achieving controlled nuclear fusion. Tokamak plasmas exhibit a variety of large scale oscillations and instabilities [1]. These range from ones which limit the plasma density or confinement time, to major disruptions which violently terminate the discharge and possibly damage the device. It is important for the design and operation of future devices to understand these plasma instabilities, especially the major disruptions. Over the last few years, resistive magnetohydrodynamic (MHD) calculations have produced a wealth of results [2–17] which have contributed substantially to the understanding of many of these features of tokamak discharges. It has even been possible to suggest ways of controlling some of the most serious plasma disruptions [13].

The resistive MHD equations, when linearized about an equilibrium, exhibit exponential solutions [18] which are driven by the gradient of the toroidal current density. They are called tearing modes because the flux surface topology is torn. However, nonlinear effects become important before the linear solutions are large enough to be experimentally measurable. The nonlinear evolution can be studied by solving the resistive MHD equations as an initial value problem. If the initial condition is that of an unstable equilibrium plus a small perturbation, then the time integration of the p.d.e.'s will first exhibit the growth rates and eigenfunctions of the

* The U.S. Government's right to retain a nonexclusive royalty-free license in and to the copyright covering this paper, for governmental purposes, is acknowledged.

† Research sponsored by the Office of Fusion Energy, U.S. Department of Energy under Contract W-7405-eng-26 with the Union Carbide Corporation.

‡ Deceased September 14, 1978.

0021-9991/81/110046–24$02.00/0

fastest growing solutions of the linearized equations. If several modes are unstable and if they have different pitches, then a three-dimensional calculation is required for the nonlinear phase. Calculations of this type have yielded results which are qualitatively distinct from the 2D results.

It is necessary to simultaneously follow phenomena on two time scales; τ_{Hp}, the transit time of an Alfvén wave in the poloidal direction; and τ_r, the resistive diffusion time of the plasma. Unfortunately, in present day tokamaks the ratio of these times is very large,

$$\tau_r/\tau_{Hp} \equiv S \sim 10^5 - 10^8,$$

and it may be even larger for reactor sized devices.

In order to understand and verify these calculations, it is necessary to clearly separate τ_{Hp}, τ_r, and the intermediate timescale characteristic of the tearing mode growth rate ($S^{1/3}\tau_{Hp}$ or $S^{2/5}\tau_{Hp}$ depending on the symmetry of the solution). This leads one to require that S to the fractional power be quite large in order to distinguish the phases and timescales of the problem in a numerical calculation. For example, it is known [19] that the exponential growth phase is followed by a nonlinear phase characterized by slower algebraic growth. It is important to show that, in certain cases, faster growth can return after a well-established period of slow algebraic growth. This is not possible for $S \lesssim 10^5$ because the algebraic growth does not have sufficient time to become clearly established. When studying the later phases of a plasma disruption at high S, it can enter a state in which the energy is no longer confined to long wavelength modes. This does not happen at low values of S and, in fact, for $S \lesssim 10^4$ some modes which are unstable at high S become stable. Also, at low S, the $p = 1$ helicity (described later) saturates, while at high S, it reconnects. For these reasons, we conclude that low S calculations are an inappropriate approach for understanding phenomena which occur at $S \sim 10^6$. On the other hand, for $S \to \infty$ the equations become singular [18]. Therefore, at high values of S the spatial structure of the solutions becomes quite small, requiring a numerical scheme capable of resolving short wavelengths in the minor radius direction. These requirements of disparate timescales and fine radial mesh imply that such calculations are time consuming even on the fastest computers available today. Consequently, execution efficiency is an important issue for any such code.

This paper primarily describes the techniques used in the code *RSF*, which was designed with the above conditions in mind. It uses a Fourier series expansion in two periodic coordinates, and a finite difference grid in the third. Its results and performance are also compared with a less efficient and less accurate three-dimensional code *RS*3 [10], and with an earlier two-dimensional code *MASS* [6]. Both of these codes use a finite difference technique. Results obtained with *RSF* have been extensively reported elsewhere [11–15], so the ones included here are merely to illustrate the capabilities of the code. An extensive review of other initial value resistive MHD calculations has been made by Schnack [20].

In Section 2 the equations and initial and boundary conditions are described. The

numerical schemes of *MASS* and *RS*3 are briefly described in Sections 3.1 and 3.2. Then in Section 3.3 a detailed description of *RSF* is given. In Section 4, a comparison of these codes is made.

2. The Equations

The full resistive MHD equations [10] (Ampere's law, Faraday's law, momentum balance, Ohm's law, equation of state, mass continuity and resistivity evolution) can be considerably simplified [10, 21] by the application of two assumptions.

The first assumption is standard tokamak (inverse aspect ratio) ordering. That is,

$$B_\theta/B_\zeta \sim \varepsilon,$$

where

$$\varepsilon \equiv a/R_o \ll 1.$$

Here a is the minor radius and R_o is the major radius of the torus. A cylindrical coordinate system (r, θ, ζ) is employed, where r $(0 \leqslant r \leqslant a)$ is the minor radius, θ $(0 \leqslant \theta \leqslant 2\pi)$ is the poloidal angle, and ζ $(0 \leqslant \zeta \leqslant 2\pi)$ is the toroidal (or longitudinal) angle. In the circular cylinder limit only terms of order ε^0 are retained and the cross-sectional shape of the plasma is assumed circular. This ordering has the important effect that the time variation of the toroidal magnetic field, B_ζ, can be ignored and, consequently, the fastest time scale of the equations, the time for the propagation of Alfvén waves across the magnetic field, is removed from the dynamics. The fastest timescale remaining in the equations is $\tau_{Hp} = R_o/V_A$, the time for Alfvén waves to propagate along the magnetic field. The slow timescale is the resistive skin time $\tau_r \equiv a^2\mu_o/\bar{\eta}$.

The second assumption is to consider only a low β plasma, where β is the ratio of plasma pressure to magnetic field pressure. Specifically, $\beta \sim \varepsilon^2$ is assumed. This is valid for most ohmically heated tokamaks.

This deliberate strategy of aiming first for efficient nonlinear, 3D, high S calculations while dropping toroidal, noncircular and finite β effects has born fruit. Even though the equations are greatly simplified, they contain the essential physics. The calculations have given quantitative agreement with a wide range of experimental observations.

The above assumptions yield two scalar partial differential equations which in dimensionless form are [10]

$$\frac{D\Psi}{Dt} = \eta J_\zeta - \frac{\partial \Phi}{\partial \zeta} - E_\zeta^W \tag{1}$$

and

$$\frac{DU}{Dt} = -S^2 \left[\hat{\zeta} \cdot (\nabla \Psi \times \nabla J_\zeta) + \frac{\partial J_\zeta}{\partial \zeta} \right], \tag{2}$$

where

Ψ is the poloidal flux function (normalized to $a^2 B_{\zeta o}$) defined by

$$\mathbf{B} = (-\varepsilon \nabla\Psi \times \hat{\zeta} + \hat{\zeta}) B_{\zeta o},$$

$\frac{D}{Dt}$ is the convective derivative $\frac{\partial}{\partial t} + \mathbf{v}_\perp \cdot \nabla$,

$\mathbf{v}$ is the fluid velocity in units of a/τ_r,

$\perp$ denotes perpendicular to $\hat{\zeta}$,

η is the resistivity normalized to unity at the magnetic axis,

$J_\zeta = \nabla_\perp^2 \Psi$ is the toroidal component of the plasma current density normalized to $\mu_o R_o / B_{\zeta o}$,

Φ is the velocity stream function, $\mathbf{v}_\perp = \nabla\Phi \times \hat{\zeta}$,

E_ζ^W is the equilibrium toroidal electric field at the wall,

$U \equiv \nabla_\perp^2 \Phi$ is the toroidal vorticity.

Most of these field quantities ($\Psi, J_\zeta, \Phi, U, \mathbf{B}_\perp$ and $\mathbf{v}_\perp$) are functions of r, θ, ζ and t. Except in Ref. [15], where the electron heat conduction equation is used to determine the resistivity η, it is assumed that

$$\eta(r) = E_\zeta^W / J_{\zeta o}(r). \tag{3}$$

This removes from the equations the resistive decay of the plasma. The electric field is taken as constant over the wall. The subscript "o" denotes an equilibrium quantity, and "$\sim$" will be used to denote the nonequilibrium ("perturbed") portion of a field quantity, for example,

$$J_\zeta \equiv J_{\zeta o} + \tilde{J}_\zeta.$$

These equations are in dimensionless form. Lengths have been normalized to the minor radius, a; and the time to τ_r.

2.1. *Initial Conditions*

The reduced equations (1), (2) have nontrivial, velocity-free equilibrium solutions for which the field quantities depend only on r. Under these conditions, the r.h.s. of Eq. (2) is zero, implying that the vorticity does not evolve. If the velocity is zero, then $\Phi_o = 0$. Since E_ζ^W cancels with $\eta J_{\zeta o}$ by definition, the r.h.s. of Eq. (1) is also zero. Since this implies that Ψ_o does not evolve, and consequently $J_{\zeta o}$ does not evolve, any such solution is an equilibrium. Equations (1) and (2) become

$$\frac{\partial}{\partial t} \Psi_o(r) = 0$$

and

$$\Phi_o = U_o = 0.$$

To specify an equilibrium, it is only necessary to specify the equilibrium poloidal flux $\Psi_o(r)$. However, it has instead been the practice to specify the safety factor $q(r)$ and then calculate the flux from

$$\frac{d}{dr}\Psi_o(r) = -\frac{r}{q(r)}. \tag{4}$$

This approach is preferable because $q(r)$ gives the positions of the resonance surfaces.

At least a dozen different parameterizations for $q(r)$ have been used, each one having from one to five independent parameters. These are useful for studying the systematic dependence of the evolution on the equilibrium. The most extensively used parameterization has been

$$q(r) = q_o[1 + (r/r_o)^{2\lambda}]^{1/\lambda}, \tag{5}$$

where

$$\lambda = \lambda_o + \tfrac{1}{2}\lambda_o'' r^2$$

and q_o, r_o, λ_o and λ_o'' are input parameters.

When profiles of the toroidal plasma current density or electron temperature are available from, e.g., transport code analyses of experimental conditions, these can be used to establish the q profile using

$$q(r) \propto \frac{r^2}{\int_o^r dr' r' J_\xi(r')} \tag{6}$$

or

$$q(r) \propto \frac{r^2}{\int_o^r dr' r' [T_e(r')]^{3/2}}. \tag{7}$$

In either case, the normalization is given by specifying q at the plasma boundary, which is directly related to the total plasma current.

The usual initial condition is zero for the velocity-related fields

$$\Phi(r, \theta, \zeta, 0) = U(r, \theta, \zeta, 0) = 0, \tag{8}$$

and an equilibrium plus a small perturbation for the poloidal flux

$$\Psi(r, \theta, \zeta, 0) = \Psi_o(r) + \tilde{\Psi}(r, \theta, \zeta), \tag{9}$$

where $\Psi_o(r)$ is given by Eq. (4).

To specify the perturbation it is useful to expand

$$\tilde{\Psi}(r, \theta, \zeta) = \sum_{m,n} [\tilde{\Psi}^c_{mn}(r) \cos(m\theta + n\zeta) + \tilde{\Psi}^s_{mn}(r) \sin(m\theta + n\zeta)]. \tag{10}$$

Note that the equilibrium is $(m = 0;\ n = 0)$ in character, so that $\Psi^s_{mn} = \tilde{\Psi}^s_{mn}$ and $\Psi^c_{mn} = \tilde{\Psi}^c_{mn}$ except for $\Psi^c_{oo} = \Psi_o + \tilde{\Psi}^c_{oo}$. The solutions of Eqs. (1) and (2) when linearized about an equilibrium are characterized by m, n values. Thus, for an equilibrium which is unstable with respect to only the $(m = 2;\ n = 1)$ mode, the quickest way to numerically approach the linear solution is to initialize $\tilde{\Psi}^c_{21}(r)$ (or $\tilde{\Psi}^s_{21}(r)$) with a function which is qualitatively similar to the linear eigenfunction, e.g.,

$$\tilde{\Psi}^c_{mn}(r) = -\left(\frac{W_I}{4}\right)^2 \frac{r^m(1-r)}{r_s^m(1-r_s)} \frac{2}{1+e^{10(-1+r/r_s)}} \frac{r_s q'}{q(r_s)^2}, \tag{11}$$

where r_s is the resonant radius of the mode, given by

$$q(r_s) = m/n,$$

and

$$q' = \left.\frac{dq}{dr}\right|_{r=r_s}.$$

The parameter W_I, the initial magnetic island width, is used to control to size of the perturbation.

Although *RSF* allows both the sine and cosine terms, in cases where only the cosine terms in Ψ are initialized, the sine terms in Ψ and the cosine terms in Φ remain zero as time evolves. In order to simplify the presentation here, only this latter situation will be discussed, therefore the superscripts "c" and "s" will be dropped.

The numerical solutions are independent of the initial perturbation if its size is sufficiently small. For a single helicity case, normally only one mode is perturbed. If the magnitude of the perturbation is sufficiently small that an eigenfunction emerges before the island width exceeds the tearing layer width, then the only role that the initial perturbation amplitude plays in the solution is to determine the zero of time. In multihelicity runs, normally two modes of differing pitch are perturbed. The solution then depends on the relative magnitudes of the two perturbations in a way which is well understood [15].

2.2. *Boundary Conditions*

The field quantities are assumed periodic in θ and ζ. At the magnetic axis, $r = 0$, all scalar functions must be regular. Later, the implementation of this in the code *RSF* is discussed.

The wall at $r = 1$ is assumed rigid, so $v_r(1) = 0$. This implies that $\Phi(1)$ is independent of θ. The constant electric field, E^W_ζ, in Eq. (1) has been chosen such that

$$\Phi(1, \theta, \zeta, t) = 0. \tag{12}$$

In Eqs. (1) and (2) Ψ contains an arbitrary additive constant, which allows us to set

$$\Psi(1, \theta, \zeta, t) = 0 \tag{13a}$$

for constant voltage, or

$$\left[\frac{d}{dr}\int d\theta\, d\zeta\, \Psi(r, \theta, \zeta, t)\right]\Bigg|_{r=1} = \text{constant} \tag{13b}$$

for constant current boundary condition.

To study the effect of external feedback coils [13] it is necessary to modify the boundary condition of the mode subject to feedback,

$$\Psi_{mn}(1, \theta, \zeta, t) = \Psi_{\text{ext}}(\theta, \zeta, t) \tag{14}$$

according to a prescription discussed in Ref. [13].

The energy conservation law for the reduced MHD equations is given by

$$\begin{aligned}\dot{\varepsilon}_M + \dot{\varepsilon}_K &= \frac{d}{dt}[\varepsilon_M + \varepsilon_K] \equiv \frac{d}{dt}\int dV\left[\frac{1}{2}(\nabla_\perp \Psi)^2 + \frac{1}{2S^2}(\nabla_\perp \Phi)^2\right] \\ &= \int \frac{\partial \Psi}{\partial t}\nabla_\perp \Psi \cdot d\mathbf{S} - \int dV\, \eta J_\zeta \tilde{J}_\zeta \equiv -F - Q,\end{aligned} \tag{15}$$

where ε_M and ε_K are magnetic and kinetic energy. Thus, the rate of change of the total plasma energy is equal to the sum of the flux through the wall and the Joule heating. The quantity

$$\delta \equiv \frac{\dot{\varepsilon}_M + \dot{\varepsilon}_K + F + Q}{\dot{\varepsilon}_M + \dot{\varepsilon}_K}$$

is used as a numerical test of energy conservation. It has proved useful to consider other approximate conservation laws, exact in the zero resistivity limit such as $\int \mathbf{A} \cdot \mathbf{B}\, dV$, where $\mathbf{A}$ is the vector potential of the magnetic field, and $\int \mathbf{v} \cdot \mathbf{B}\, dV$.

3. Numerical Schemes

It is necessary to integrate Eqs. (1) and (2) in time starting from a perturbed equilibrium. Three techniques to do this will be described in chronological order. The first two have been described elsewhere [6, 10], so only sufficient detail is given here to allow comparison with the technique used in code *RSF*.

Lagrangian and partly Lagrangian schemes have been found useful for solving other fluid problems [22]. However, the driving terms in Eqs. (1) and (2) come from the magnetic field, so the analogous choice would be a finite difference grid which

evolves with the magnetic field. But this choice is excluded in resistive MHD because the magnetic field topology changes due to the magnetic islands, and in some cases, the field lines wander stochastically. The most straightforward Eulerian coordinate system would be Cartesian, which has been applied in other circumstances [23, 24]. However, since at low resistivity the tearing layer is highly localized in terms of the magnetic flux coordinate, such a coordinate system provides the most accurate representation of the tearing layer. In circular cylinder geometry, the minor radius, r, is an equilibrium flux coordinate. Since, as stated above, the total flux does not provide a useful coordinate, an unequal-spaced finite difference grid in minor radius is the best choice. The following sections present different ways of representing variations in θ and ζ.

3.1. *Helical Symmetric Case*

The *MASS* code was developed by the joint effort of the resistive MHD groups in Princeton at the Princeton Plasma Physics Laboratory and the Institute for Advanced Studies [2, 4, 5]. It was later modified and extensively used at ORNL [7, 9]. It is summarily described here only to give better perspective to the other techniques.

The terms in Eq. (10) can be grouped by helicity. If $p \equiv m/n$, then the double sum can be restated

$$\tilde{\Psi}(r, \theta, \zeta, t) = \sum_p \sum_n \tilde{\Psi}_{np,n}(r, t) \cos[(p\theta + \zeta)n], \tag{16}$$

where p takes all rational values. If only perturbations of a single pitch (or helicity), p, are initialized, then, in cylindrical geometry, where the equilibrium is ($m = 0$; $n = 0$), other helicities are never generated. The problem is thus reduced to two spatial dimensions, r and $\theta_p \equiv p\theta + \zeta$.

The *MASS* code was developed to study these single helicity cases. It played a crucial role in analyzing both linear and nonlinear behavior of tearing modes. It was used to study the $p = 1$ helicity as a model for sawtooth oscillations [7]. Calculations for other helicities ($p \neq 1$) show a period of exponential growth followed by saturation of the perturbation giving a new stable nonaxisymmetric final state. When S is large ($\sim 10^6$), there is a well-defined period prior to island saturation in which the perturbation slows from exponential growth to algebraic growth. This numerically supports the result of Rutherford [19].

The *MASS* code uses a finite difference formulation on a 2D polar grid in r and θ_p. Because of symmetry, it is only necessary to employ a segment of the grid such that

$$0 \leqslant \theta_p \leqslant \pi/m_{\min}.$$

However, to get answers which are even qualitatively good can require about 20 grid points in the θ_p direction (Figs. 1 and 2).

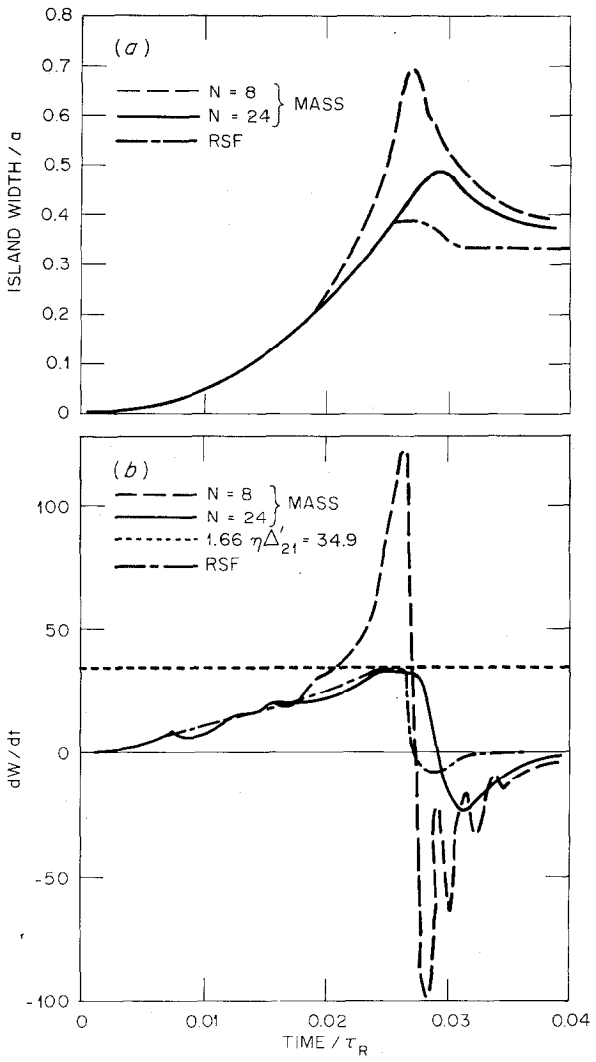

FIG. 1. The island width, W, is shown as a function of time (a) for the *MASS* code with 8 and 24 points in the θ_p grid. This is a typical $p = 2$ saturating island. When the grid is too coarse ($N = 8$) there is a severe overshoot in island width. As N is increased, the *MASS* code results approach the *RSF* results. In the coarse grid case, $N = 8$, the time derivative of the width (b) considerably exceeds the estimate which comes from a Δ' calculation.

The *MASS* code cannot correctly calculate the evolution of equilibria which are strongly unstable to more than one helicity since it does not include any nonlinear effects between modes of unequal helicity. A three-dimensional code, *RS*3, was developed to study these effects.

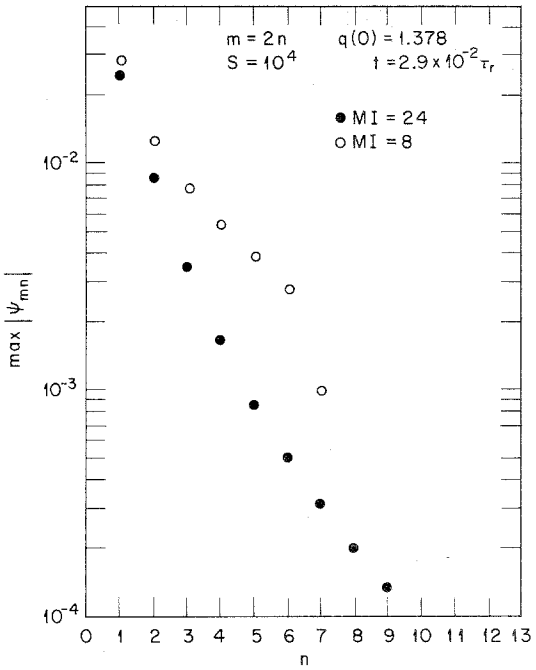

FIG. 2. The maximum absolute value of the amplitude of Ψ_{mn} is plotted as a function of n for the single helicity $p = 2$ *MASS* code runs shown in Fig. 1. The values shown were taken at a time corresponding to the peak in the island width. For the coarse grid run ($N = 8$), the higher n modes are poorly resolved resulting in anomalously large values of $|\Psi_{mn}|$.

3.2. *Cylindrical Finite Difference Grid Technique*

The generalization to three dimensions to allow for the interaction of different helicities was accomplished in *RS*3 by replacing the polar grid of the *MASS* code with a full cylindrical grid. In cases where only one helicity is unstable or in which the unstable modes saturate at a sufficiently low level, *RS*3 duplicates the results of the *MASS* code. However, when more than one mode is unstable, and when the single helicity saturation amplitudes are sufficiently large, the behavior departs from a superposition of single helicity solutions, and a qualitatively different solution is found.

From linear tearing mode theory [18], it is known that the resistivity plays a role only inside the tearing layer, which is a very narrow region surrounding the singular radius. The tearing layer width ε_T is proportional to $S^{-2/5}$. One expects, therefore, that a very fine radial grid is required, at least in the vicinity of the singular surfaces of unstable modes. In addition to this, the θ and ζ grids must be fine, not only to support a sufficient number of m and n values, but also to minimize a sensitive form of truncation error. Consider any function of the form

$$f = \cos(m\theta + n\zeta). \tag{17}$$

The finite difference first derivative on an equal-spaced grid is given by

$$\frac{\delta f}{\delta \zeta} = -n[1 - (n\,\Delta\zeta)^2/6]\,\sin(m\theta + n\zeta) + O((\Delta\zeta)^4) \tag{18}$$

and similarly for the θ-derivative.

The discretization error,

$$n_{\text{eff}}/n = 1 - (n\,\Delta\zeta)^2/6, \tag{19}$$

occurs in any term with a ζ or θ derivative. These factors reduce the contribution of the higher modes in such terms. The solutions are particularly sensitive to driving terms of the form

$$\frac{\delta f}{\delta \zeta} - \frac{1}{q}\frac{\delta f}{\delta \theta}. \tag{20}$$

Such terms should go to zero at the resonant surface where $q = m/n$. This will be the case if the grid is chosen such that

$$\frac{m_{\text{eff}}}{n_{\text{eff}}} = q, \tag{21}$$

which implies that $n\,\Delta\zeta = m\,\Delta\theta$. Even the elimination of this part of the discretization error is only effective for a single helicity at a time, and the discretization error still appears in some nonlinear terms. In order to overcome these problems and the fact that *RS*3 is too slow to be useful in systematic studies, *RSF* was written.

3.3. *Fourier Series Expansion Technique*

To overcome the limitation due to discretization in the θ and ζ directions, *RSF* is designed to use a Fourier series expansion in these two directions. Each of the field quantities is expanded as in Eq. (10), a finite set of terms is retained, and the amplitudes of each mode are discretized on an unequally spaced grid in minor radius

$$\Psi_{mn}(r) \to \Psi_{mn}(r_j) \qquad j\colon 1,\ldots,J.$$

RSF has confirmed, with greater efficiency, the multiple helicity results of *RS*3 (Fig. 3) and the single helicity results of the *MASS* code (Fig. 1).

As long as the solution is dominated by a moderate number of $(m; n)$ modes, this representation is considerably more natural and economical than grids in θ and ζ. This certainly holds in the early stages of a calculation where very low mode numbers dominate. In the later stages of some multihelicity calculations short wavelength components of the solution become important. Beyond a certain point, both finite difference and finite series representations become inadequate.

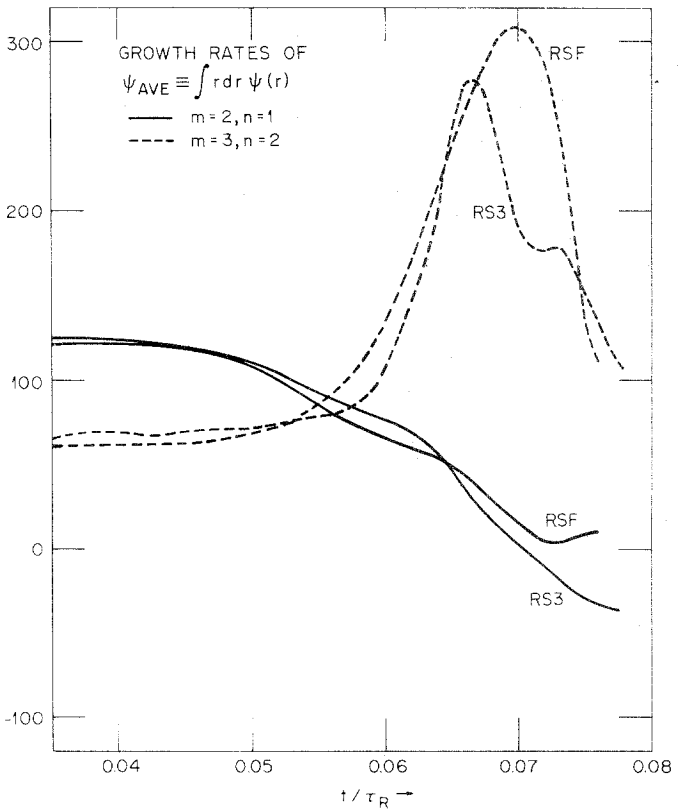

FIG. 3. In the nonlinear regime, the instantaneous growth rate of the $(m = 3; n = 2)$ mode exhibits a strong peak just after the $p = 3/2$ island overlaps with the $p = 2$ island. There is rough quantitative agreement between *RS*3 and *RSF* through this phase of the calculation.

3.3.1. *Equations.* As in Ref. [10], a two-step algorithm is proposed:

$$U^{t+\Delta t/2} = U^t + \frac{\Delta t}{2} S_1, \tag{22a}$$

$$\tilde{\Psi}^{t+\Delta t/2} = \tilde{\Psi}^t + \frac{\Delta t}{2} S_2, \tag{22b}$$

$$U^{t+\Delta t} = U^t + \Delta t\, S_3, \tag{22c}$$

$$\tilde{\Psi}^{t+\Delta t} = \tilde{\Psi}^t + \Delta t\, S_4. \tag{22d}$$

The four source terms, S_i, are determined from Eqs. (1) and (2) with the constraints that

(1) S_3 and S_4 are evaluated at $t + \Delta t/2$ to give a second order accurate timestep. This gives a controllable global error of order Δt.

(2) All nonlinear terms are evaluated explicitly to avoid solving very large matrix problems.

To determine the best time-level for evaluating the terms in S_1 and S_2, a numerical [illegible] solution not be allowed to grow. If both S_1 and S_2 are evaluated at time t, then the numerically stable timestep is controlled by radial grid spacing. Since dense radial grids are needed, this restriction is very costly. This can be avoided by taking the ηJ_ζ term in S_2 at $t + \Delta t/2$. Numerical tests have confirmed this.

The result is

$$S_1 = \nabla_r \Phi^t \nabla_\theta U^t - \nabla_\theta \Phi^t \nabla_r U^t - S^2 \left\{ \frac{1}{q} \left[-r \nabla_\theta \tilde{J}_\zeta^t + q \frac{\partial}{\partial \zeta} \tilde{J}_\zeta^t \right] - \nabla_\theta \tilde{\Psi}^t \frac{d}{dr} J_{\zeta o} + \nabla_r \tilde{\Psi}^t \nabla_\theta \tilde{J}_\zeta^t - \nabla_r \tilde{J}_\zeta^t \nabla_\theta \tilde{\Psi}^t \right\}, \tag{23}$$

$$S_2 = \frac{r}{q} \nabla_\theta \Phi^t - \frac{\partial}{\partial \zeta} \Phi^t + \eta \tilde{J}_\zeta^{t+\Delta t/2} - \nabla_r \tilde{\Psi}^t \nabla_\theta \Phi^t + \nabla_\theta \tilde{\Psi}^t \nabla_r \Phi^t, \tag{24}$$

$$S_3 = \nabla_r \Phi^{t+\Delta t/2} \nabla_\theta U^{t+\Delta t/2} - \nabla_\theta \Phi^{t+\Delta t/2} \nabla_r U^{t+\Delta t/2} - S^2 \left\{ \frac{1}{q} \left[-r \nabla_\theta \tilde{J}_\zeta^{t+\Delta t/2} + q \frac{\partial}{\partial \zeta} \tilde{J}_\zeta^{t+\Delta t/2} \right] - \nabla_\theta \tilde{\Psi}^{t+\Delta t/2} \frac{d}{dr} J_{\zeta o} + \nabla_r \tilde{\Psi}^{t+\Delta t/2} \nabla_\theta \tilde{J}_\zeta^{t+\Delta t/2} - \nabla_r \tilde{J}_\zeta^{t+\Delta t/2} \nabla_\Theta \tilde{\Psi}^{t+\Delta t/2} \right\}, \tag{25}$$

$$S_4 = \frac{r}{q} \nabla_\theta \Phi^{t+\Delta t/2} - \frac{\partial}{\partial \zeta} \Phi^{t+\Delta t/2} + \eta \tilde{J}_\zeta^{t+\Delta t/2} - \nabla_r \tilde{\Psi}^{t+\Delta t/2} \nabla_\theta \Phi^{t+\Delta t/2} + \nabla_\theta \tilde{\Psi}^{t+\Delta t/2} \nabla_r \Phi^{t+\Delta t/2}, \tag{26}$$

where

$$U \equiv \frac{1}{r} \nabla_r (r \nabla_r \Phi) + \nabla_\theta^2 \Phi \tag{27}$$

and

$$J_\zeta \equiv \frac{1}{r} \nabla_r (r \nabla_r \Psi) + \nabla_\theta^2 \Psi, \tag{28}$$

and where

$$\nabla_\theta \equiv \frac{1}{r} \frac{\partial}{\partial \theta}$$

and

$$\nabla_r \equiv \frac{\partial}{\partial r}.$$

Each of the field quantities in Eqs. (22)–(28) ($U, \Phi, \tilde{J}_\zeta, \tilde{\Psi}$) is then expanded as in Eq. (10). Each equation is multiplied by $\cos(m\theta + n\zeta)$ or $\sin(m\theta + n\zeta)$ and integrated with respect to θ and ζ. This has the effect of projecting out a single mode on the left-hand side of Eq. (22). The mode numbers for linear source terms agree with the quantity being advanced, e.g.,

$$\frac{\Psi_{mn}^{t+\Delta t/2} - \Psi_{mn}^{t}}{\Delta t/2} = \frac{r}{q}\nabla_\theta \Phi_{mn}^{t} + \cdots.$$

If a total of L modes are included in the calculation, then in each half of the step, there are $2L$ equations to be advanced. Each of the 12 nonlinear terms becomes a convolution of amplitudes, e.g.,

$$\frac{U_{mn}^{t+\Delta t/2} - U_{mn}^{t}}{\Delta t/2} = \sum_{\substack{m'n' \\ m''n''}} F_{m'n'm''n''}^{mn} \nabla_r \Phi_{m'n'}^{t} \nabla_\theta U_{m''n''}^{t} + \cdots, \tag{29}$$

where F is a sparse matrix whose elements have values $\pm 1, 0$.

For each timestep, three tridiagonal matrix problems must be solved:

for Φ^t using Eq. (27),

for $\Psi^{t+\Delta t/2}$ (due to the $\eta \tilde{J}_\zeta^{t+\Delta t/2}$ term) in Eq. (24),

for $\Phi^{t+\Delta t/2}$ using Eq. (27).

These are not a very time-consuming part of the timestep.

In *RSF*, Eqs. (22)–(28) are solved using the boundary conditions stated earlier. It has not been necessary to employ any techniques to suppress numerical difficulties. Except in the most pathological cases, the code has performed quite accurately. In cylindrical geometry the origin ($r = 0$) can sometimes be numerically difficult to treat. Such difficulties are avoided here because all functions are scalar (rather than vector or tensor) fields, and because regularity at the origin is particularly easy to impose in terms of individual modes. For $m \neq 0$ components, the scalar functions must go to zero at $r = 0$. For $m = 0$ components, the first derivative with respect to r must vanish at $r = 0$.

The entire calculation is carried out in terms of the modes (Ψ_{mn}, U_{mn}, etc.). Fourier transformations back to (r, θ, ζ)-space are used only for generating certain types of output, never in the solution of the partial differential equations themselves.

3.3.2. *Choice of Modes.* Cases in which only a single mode is initially perturbed are called single helicity cases. This is due to the fact that the nonlinear terms

generate only modes of the same helicity, $p = m/n$, as the perturbed mode. Thus, Eq. (10) reduces to

$$\Psi(r, \theta, \zeta, t) = \Psi_{o,o}(r) + \sum_{n=n_{\min}}^{\infty} \Psi_{np,n}(r) \cos[(p\theta + \zeta)n]. \tag{30}$$

It is necessary to truncate the series at some finite value $n = N$. Single helicity calculations have two general types of nontrivial solutions. In saturation cases, the solution goes to a time-independent final state in such a way that the magnitudes of the amplitudes drop off rapidly with n at all times during the calculation [9]. The second class of single helicity cases, where magnetic reconnection occurs, results in a time-independent final state dominated by the $(m = 0; n = 0)$. However, during part of the evolution, it is necessary to include a substantial number of modes. In either case, the number of modes required in *RSF* is considerably smaller than the number of grid points required in the *MASS* code (Figs. 1 and 4).

For multihelicity cases, in which modes of unequal helicity are perturbed, the choice of modes is not so simple. One could argue that the only criterion should be to keep modes of long wavelength. This suggests a condition such as

$$n \leqslant N \qquad \text{and} \qquad m \leqslant M \tag{31a}$$

or perhaps

$$n^2 + m^2 \leqslant M^2 + N^2. \tag{31b}$$

Experience has shown that these are very inefficient choices because they include many unimportant modes. There is a tendency for the modes which are not resonant, for which $p = m/n$ does not equal $q(r)$ anywhere in the plasma, to be unimportant.

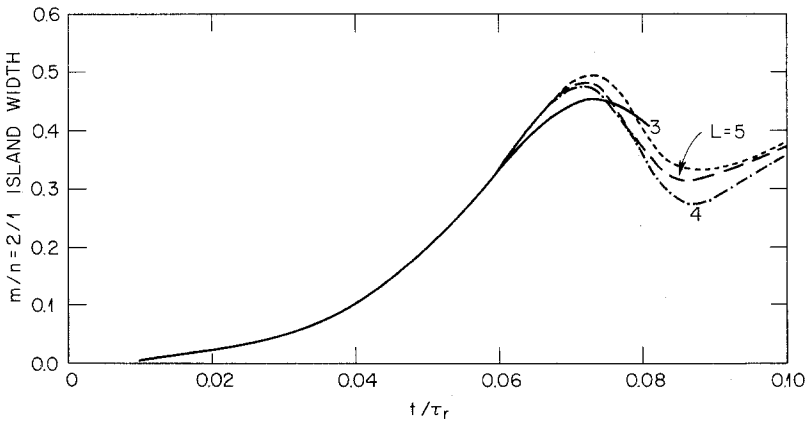

FIG. 4. Single helicity $(m/n = 2)$ case. The time dependence of the island width converges rapidly with the number of modes in *RSF*. The solid, dot–dashed, and long dashed curves correspond to the mode selections 0/0 2/1 4/2 $(L = 3)$, 0/0 2/1 4/2 6/3 $(L = 4)$, and 0/0 2/1 4/2 6/3 8/4 $(L = 5)$, respectively. The short dashed line is the *MASS* code result with $MI = 24$.

During the early stages of evolution the one or two modes which are linearly unstable completely dominate. Considering this, an ad hoc ordering scheme has been devised which can be used to determine an efficient choice of modes. Consider a case in which the $(m = 2;\ n = 1)$ and $(m = 3;\ n = 2)$ modes are linearly unstable, and with the $(m = 2;\ n = 1)$ significantly larger than the $(m = 3;\ n = 2)$ mode throughout the calculation. Assume that

$$\Psi_{00} \sim 1,$$
$$\Psi_{21} \sim \delta,$$

and

$$\Psi_{32} \sim \delta^2,$$

where δ is a small parameter.

When two modes interact, they directly generate modes which have mode numbers which are the sum and difference;

$$(m_1; n_1) \text{ and } (m_2; n_2) \text{ directly}$$
$$\text{generate } (m_1 + m_2; n_1 + n_2) \text{ and } (m_1 - m_2; n_1 - n_2).$$

This leads to the following ordering

$O(\delta^0)$: $\Psi_{0,0}$

$O(\delta^1)$: $\Psi_{2,1}$

$O(\delta^2)$: $\Psi_{3,2}$ $\Psi_{4,2}$

$O(\delta^3)$: $\Psi_{1,1}$ $\Psi_{5,3}$ $\Psi_{6,3}$

$O(\delta^4)$: $\Psi_{1,0}$ $\Psi_{6,4}$ $\Psi_{7,4}$ $\Psi_{8,4}$

$O(\delta^5)$: $\Psi_{3,1}$ $\Psi_{4,3}$ $\Psi_{8,5}$ $\Psi_{9,5}$ $\Psi_{10,5}$

$O(\delta^6)$: $\Psi_{2,2}$ $\Psi_{5,2}$ $\Psi_{9,6}$ $\Psi_{10,6}$ $\Psi_{11,6}$ $\Psi_{12,6}$

$O(\delta^7)$: $\Psi_{0,1}$ $\Psi_{7,3}$ $\Psi_{7,5}$ $\Psi_{11,7}$ $\Psi_{12,7}$ $\Psi_{13,7}$ $\Psi_{14,7}$

...

It is natural to truncate this series at some order, thus choices of 7, 11, 16, 22 or 29 modes are reasonable. Runs have been made with up to 79 modes.

Although "ordering pyramids," like that above, have been remarkably successful in predicting the modes which are important for numerical calculations, they in no way constitute a proof that other modes are not important. This must be tested by making runs with different selections of modes.

To produce Fig. 5, the modes $0 \leqslant n \leqslant 5$, $0 \leqslant m \leqslant 5$ were used. The magnetic energy of each mode was determined late in the run. Modes for which $-\log$ M.E. is

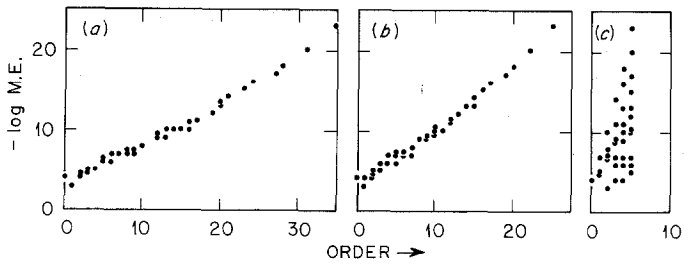

FIG. 5. For a 36 mode *RSF* case, the magnetic energy is plotted as a function of "order." "Order" has been assigned to the 36 modes according to three different ad hoc schemes. In (a) there is the strongest correlation between "order" and magnetic energy. In (c) the "order" is a very poor predictor of the importance of a mode.

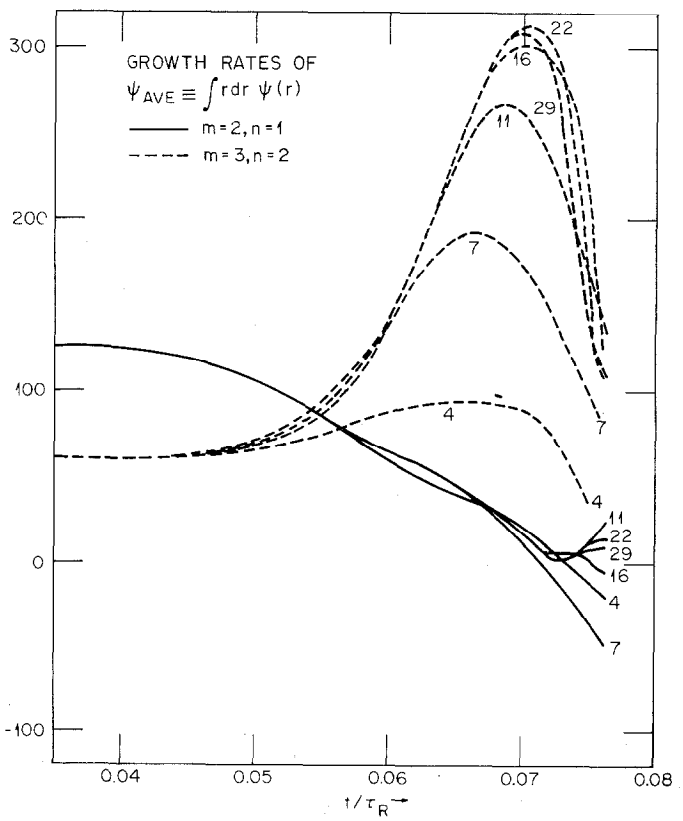

FIG. 6. The solution obtained with *RSF* converges rapidly as the number of modes is increased. Modes here were based on the ordering pyramid in the text. In this type of multihelicity run, smaller wavelengths become important as time goes on. Thus, the addition of more modes merely postpones the onset of numerical error.

large are relatively unimportant. Each of the 36 modes is assigned an order according

(a) the ordering pyramid above;

(b) as above, but assuming $\Psi_{3,2} = O(\delta^1)$ and modifying the pyramid accordingly;

(c) setting the order to $\min(m, n)$.

The whole purpose of the ordering scheme is to have a reasonably good predictor of mode importance. Figure 5 shows that for this case scheme (a) is the best predictor of mode size. Scheme (b) is slightly worse, and scheme (c) shows only slight correlation between order and mode size. When the ordering pyramid is employed, the convergence of the solution with number of modes is rapid (Fig. 6).

With *RSF* it is possible to exclude individual modes selectively in order to assess their importance. This facility has proved useful in understanding major disruption cases [15]. In a pure finite difference scheme, such as *RS*3, this technique cannot be used. *RSF* also has the advantage that the linear behavior of high numbered modes can be studied inexpensively and accurately.

When the n values of the modes in a calculation are multiplied by a positive integer, I, and $q \to q/I$, then the solutions are unchanged. This is a necessary property for the solutions to possess and has provided a check against certain programming errors.

3.3.3. *Convolution.* Each timestep requires 12 convolutions (Eq. (29)). This is the most time-consuming part of the calculation. If the total number of modes is L and the number of radial grid points is J, then, for each of the 12 convolutions there are $L \times J$ possible left-hand sides. For each of these, the summation will have on the order of L nonzero terms. Since each calculation requires a large number ($\sim 10^3$ to $\sim 10^5$) of timesteps, it is desirable to set up as much of the convolution as possible at the start of the run. Assume, in Eq. (29), that the derivatives have been done, giving

$$R_{mn} = \sum_{\substack{m'n' \\ m''n''}} F^{mn}_{m'n'm''n''} G_{m'n'} H_{m''n''}, \tag{32}$$

where the summation includes only the terms chosen by the ordering scheme. Further, assume that the set of modes included in the run forms an ordered list:

$$(m_l; n_l) \qquad l = 1, 2, \ldots, L.$$

Each mode can be identified by an l subscript, rather than the double m, n notation:

$$R_l = \sum_{l', l''} F^l_{l'l''} G_{l'} H_{l''}. \tag{33}$$

At the start of a run two subscripts arrays (g and h) are prepared, allowing the convolution to take the form

$$R_l = \sum_{i=1}^{I_l} G_{g_{li}} H_{h_{li}}.$$

This technique avoids all of the zero contributions to the convolution. Unfortunately, this style of loop is very inefficient on the *CRAY*-1 computer because it involves nonlinear subscripts. Since nearly all of the production running of *RSF* has been on a *CRAY*-1, it is worthwhile to look for another way to do the convolution. Each of the field quantities is stored as, e.g., Ψ_{jl}, where j labels the grid point, and l labels the mode. Since the convolution operation must be done at each grid point, the j loop can be brought inside, giving

$$R_{jl} = \sum_{i=1}^{I_l} G_{jg_{li}} H_{jh_{li}}.$$

This generates very efficient vector code on the *CRAY*-1.

3.3.4. *Timestep.* The numerical stability analysis referred to in Section 3.3.1 gives the timestep size for numerical stability

$$\Delta t_0 \leqslant \frac{2}{S \operatorname{Max} |n - m/q|}, \tag{34}$$

where the Max is over all $(m; n)$ pairs in the calculation and over all values of q in the plasma. Runs with high values of m and n require a smaller timestep. This is analogous to the dependence on grid spacing in the *MASS* code and in *RS*3. However, the spacing in minor radius does not appear in Eq. (34) since the ηJ_ζ term is implicit. This is fortunate, since in many cases $\Delta r \lesssim 0.003$.

The initial timestep size is given as a fraction of Δt_o so that the initial timestep is somewhat smaller than required by the stability analysis. As nonlinear effects become important, it sometimes proves necessary to reduce the timestep. A procedure for doing so during a run has been developed. It has a rather weak theoretical basis, but in practice it works quite well. When a numerical instability starts to grow, it can usually be seen as a short wavelength oscillation in the modes. To detect the oscillation early in its development, it is advisable to look at a sensitive quantity. J_ζ is more sensitive to the numerics than is Ψ since J_ζ is the second derivative of Ψ. Since $(J_\zeta)_{00}$ is always present, we choose that component. In particular, whenever the number of oscillations (as a function of r) of $(J_\zeta)_{00}$ increases, the timestep is reduced by a factor which is usually set to 0.8. There certainly are some cases in which this fails, usually by unnecessarily lowering the timestep, but in most cases this procedure works well.

A code, *RSFMOL*, has been developed in which the above timestepping procedure is replaced with a method of lines technique [25]. Several standard ODE solvers

which determine their own timesteps have been invoked [26]. This appears to be an expensive technique which only pays for itself very late in a run where, using our standard technique, the timestep has been unnecessarily reduced.

3.3.5. *Grid.* Tearing modes are localized in minor radius. This localization becomes more severe at high values of S and/or m. Our initial value codes allow a nonuniform grid to be specified. In single helicity cases, this can be put to significant advantage by placing a high density of points near the resonant surface. For multihelicity cases with many resonant surfaces the advantage is considerably reduced. Often such runs are made with uniform grids. The finite difference formulas for first and second derivatives are 3-point formulas which take unequal spacing into account.

3.3.6. *Sources of Numerical Error.* There are five sources of numerical error:

(1) Truncation of the infinite sum of modes;

(2) Truncation error due to the finite grid in r;

(3) Truncation error due to finite timestep;

(4) Roundoff error;

(5) Numerical instability.

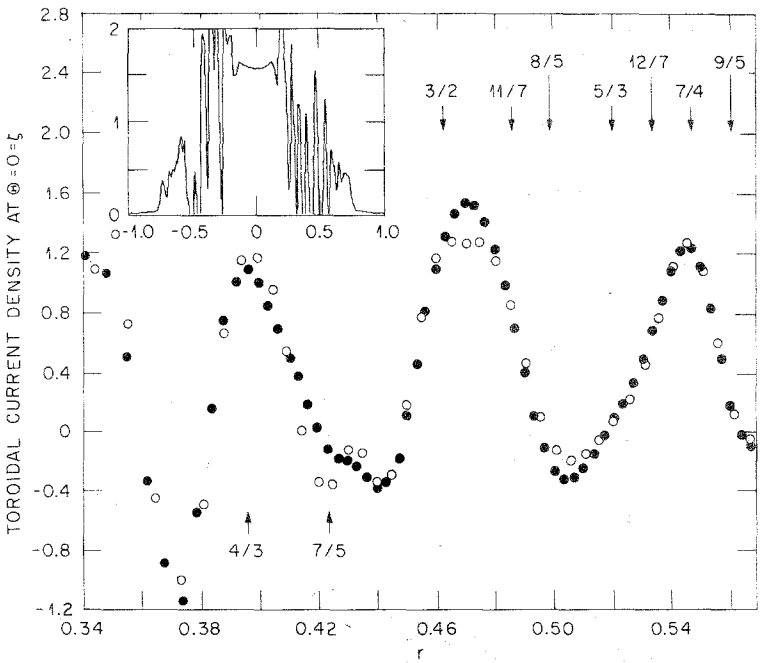

FIG. 7. The toroidal current density viewed across a plasma diameter (inset) exhibits fine scale oscillations. The radial grid must be chosen sufficiently fine to accurately resolve them. A close inspection shows that grid densities of the order of 200 radial points are sufficient. The oscillations are seen to be insensitive to the locations of grid points.

For single- or multihelicity cases in which islands saturate, convergence of the solution with respect to the number of modes, L, is very rapid (Fig. 4). Normally, the solution is well converged with about five modes per unstable helicity, showing that long wavelength behavior dominates throughout the evolution. In those particular cases where there is an interaction between different helicities, there is a transfer of energy from long wavelengths to shorter wavelengths which occurs at the very end of the calculation. This is apparent in Fig. 6, where it can be observed that when fewer modes are used, the solution breaks down sooner. This pattern holds for as many modes (79) as we have used. In any event, for a given number of modes, there is a time at which the calculation must be stopped. Presumably, the energy will continue to flow into shorter wavelengths. Eventually, the fluid model breaks down. If one wished to continue, then a different approach, suited to a turbulent configuration, would be needed.

At small values of S ($S \simeq 10^4$) 100 to 200 grid points are adequate while, at $S \simeq 10^6$, 200 to 300 points are usually needed. This corresponds to $\Delta r \simeq 10^{-3}$ in the vicinity of important singular surfaces. It is necessary to run a case with at least two different grid sizes to verify the result. The inset in Fig. 7 shows the toroidal current, J_t, late in a run at $S = 10^5$. An enlargement of the region with small wavelength oscillations shows that the spikes are real; they are well reproduced on two different grids. The magnetic island width of the ($m = 3$; $n = 2$) mode is rather sensitive to numerical error. It is plotted in Fig. 8 as a function of time for several grid sizes, again at $S = 10^5$. Convergence to the solution is quite evident.

One test of the level of numerical dissipation has been to observe the dependence of linear growth rate on the level of resistivity, S [16, 27]. The numerical dissipation is so small that the growth rate exhibits the theoretical value for S up to at least 10^7

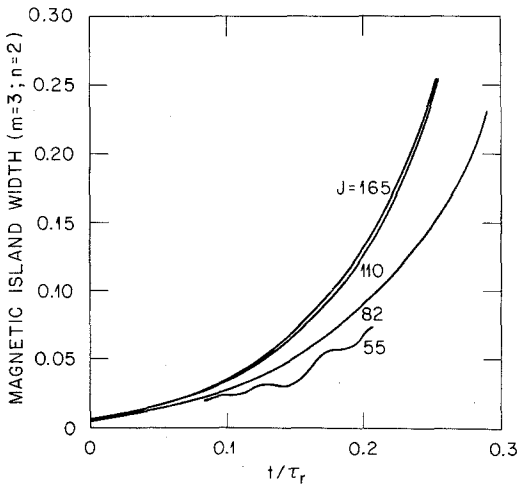

FIG. 8. The $p = 3/2$ magnetic island width becomes independent of radial grid density for $J \gtrsim 100$.

Within the numerical stability constraint of Eq. (34), the timestep has been varied to see the effects of the finite difference expression for the time derivative. No detectable effects have been seen. Evidently, numerical stability is a more restrictive constraint.

RSF is normally run in single precision on the *CRAY*-1. Floating point format uses 48 bits (14^+ decimal digits) for the mantissa. There is a compiler option to select a shorter mantissa. This feature has been used to verify that roundoff error is insignificant.

The control of numerical instability is accomplished in the ad hoc fashion described in Section 3.3.4. If the initial timestep is too large, there is a sharp onset of short wavelength numerical oscillations. It is presumed that the absence of such oscillations indicates the lack of significant numerical instability.

4. Comparison of Codes

The reduced MHD Eqs. (1) and (2) have been solved with several different techniques by the authors. In their common region of validity, the nonlinear initial value codes, *MASS*, *RS*3, *RSFMOL* and *RSF* agree when properly converged. In turn, these results agree with linear growth rates and approximate saturation island widths obtained from Δ' calculations [28]. When only these two pieces of information are desired, the Δ' calculation is the method of choice, since it is more efficient than the initial value techniques. Both techniques can be adapted to somewhat more general geometries [16, 27]. The Δ' calculation provides a check of the linear growth rates in this situation and can also contribute to the understanding of the initial value results. Of the initial value codes, *RSF* is by far the fastest. The other codes are normally run only to verify the *RSF* results.

5. Conclusions

An efficient technique for solving the nonlinear reduced MHD equations has been developed. Using cylindrical coordinates, the functions are represented by Fourier series expansions in the two periodic coordinates and a finite difference grid in the third direction. This technique has been verified by comparison with earlier results and is more efficient and removes some inherent problems of the finite difference method. It also has a larger domain of applicability which makes it possible to do systematic 3D nonlinear studies of the stability of plasmas to resistive MHD modes for low values of the resistivity. This approach also gives high flexibility to the calculations and allows the testing of different dynamical hypotheses by the convenient selection of modes.

REFERENCES

1. E. P. GORBUNOV *et al.*, *At. Energy* **15** (1963), 363 [*Sov. At. Energy* **15** (1963), 1105]; L. A. ARTSIMOVICH *et al.*, *At. Energy* **17** (1964), 170 [*Sov. At. Energy* **17** (1964); 886]; L. A. ARTSIMOVICH *et al.*, *in* "Plasma Physics and Controlled Nuclear Fusion Research," Vol. I, p. 443, International Atomic Energy Agency, Vienna, 1971; S. VON GEOLER *et al.*, *Phys. Rev. Lett.* **33** (1974), 1201; V. S. VLASENKOV *et al.*, *Nuclear Fusion Suppl.* **1** (1975), 1; L. A. BERRY *et al.*, *in* "Plasma Physics and Controlled Nuclear Fusion Research," Vol. I, p. 49, International Atomic Energy Agency, Vienna, 1977; I. HUTCHINSON, *Phys. Rev. Lett.* **37** (1976), 388; D. B. ALBERT *et al.*, *Nuclear Fusion* **17** (1977), 863; S. V. MIRNOV *et al.*, *in* "Plasma Physics and Controlled Nuclear Fusion Research," Vol. I, p. 291, International Atomic Energy Agency, Vienna, 1977; N. R. SAUTHOFF *et al.*, *Nuclear Fusion* **18** (1978), 1445; K. TOI, S. ITOH, K. KADOTA, K. KAWAHATA, N. NODA, K. SAKURAI, K. SATO, S. TANAHASHI, AND S. YASUE, *Nuclear Fusion* **19** (1979), 1643.
2. B. V. WADDELL *et al.*, *Nuclear Fusion* **16** (1976), 528.
3. D. BISKAMP AND H. WELTER, *in* "Plasma Physics and Controlled Nuclear Fusion Research," Vol. I, p. 579, International Atomic Energy Agency, Vienna, 1977.
4. R. B. WHITE *et al.*, *in* "Plasma Physics and Controlled Nuclear Fusion Research," Vol. I, p. 569, International Atomic Energy Agency, Vienna, 1977.
5. R. B. WHITE, D. A. MONTICELLO, M. N. ROSENBLUTH, AND B. V. WADDELL, *Phys. Fluids* **20** (1977), 800.
6. B. V. WADDELL, M. N. ROSENBLUTH, D. A. MONTICELLO, R. B. WHITE, AND B. CARRERAS, *in* "Theoretical and Computational Plasma Physics," p. 79, International Atomic Energy Agency, Vienna, 1978.
7. G. L. JAHNS, M. SOLER, B. V. WADDELL, J. D. CALLEN, AND H. R. HICKS, *Nuclear Fusion* **18** (1978), 609; B. V. WADDELL, G. L. JAHNS, J. D. CALLEN, AND H. R. HICKS, *Nuclear Fusion* **18** (1978), 735.
8. B. V. WADDELL, B. CARRERAS, H. R. HICKS, J. A. HOLMES, AND D. K. LEE, *Phys. Rev. Lett.* **41** (1978), 1386.
9. B. CARRERAS, B. V. WADDELL, H. R. HICKS, AND S. J. LYNCH, *Phys. Rev. A* **18** (1978), 735.
10. B. V. WADDELL, B. CARRERAS, H. R. HICKS, AND J. A. HOLMES, *Phys. Fluids* **22** (1979), 896.
11. B. CARRERAS, B. V. WADDELL, AND H. R. HICKS, *Nuclear Fusion* **19** (1979), 1423.
12. J. D. CALLEN, B. V. WADDELL, B. CARRERAS, M. AZUMI, P. J. CATTO, H. R. HICKS, J. A. HOLMES, D. K. LEE, S. J. LYNCH, J. SMITH, M. SOLER, K. T. TSANG, AND J. C. WHITSON, *in* "Plasma Physics and Controlled Nuclear Fusion Research," Vol. I, p. 415, International Atomic Energy Agency, Vienna, 1979.
13. J. A. HOLMES, B. CARRERAS, H. R. HICKS, S. J. LYNCH, AND B. V. WADDELL, *Nuclear Fusion* **19** (1979), 1333.
14. B. CARRERAS, H. R. HICKS, AND B. V. WADDELL, *Nuclear Fusion* **19** (1979), 583.
15. B. CARRERAS, H. R. HICKS, J. A. HOLMES, AND B. V. WADDELL, *Phys. Fluids* **23** (1980), 1811.
16. B. CARRERAS, H. R. HICKS, AND D. K. LEE, *Phys. Fluids* **24** (1981), 66.
17. H. R. HICKS, B. A. CARRERAS, J. A. HOLMES, D. TETREAULT, G. BERGE, J. P. FREIDBERG, AND P. A. POLITZER, *in* "Plasma Physics and Controlled Nuclear Fusion Research," Vol. I, p. 259, International Atomic Energy Agency, Vienna, 1981.
18. H. P. FURTH, J. KILLEEN, AND M. N. ROSENBLUTH, *Phys. Fluids* **6** (1963), 459.
19. P. H. RUTHERFORD, *Phys. Fluids* **16** (1973), 1903.
20. D. SCHNACK AND J. KILLEEN, *J. Comp. Phys.* **35** (1980), 110.
21. H. R. STRAUSS, *Phys. Fluids* **19** (1976), 134.
22. J. U. BRACKBILL, *in* "Methods in Computational Physics" (J. Killeen, Ed.), Vol. 16, p. 1, Academic Press, New York, 1976.
23. A. SYKES AND J. A. WESSON, *Phys. Rev. Lett.* **37** (1976), 140.
24. H. R. HICKS AND J. W. WOOTEN, *Comput. Phys. Comm.* **13** (1977), 117.
25. P. W. GAFFNEY, H. R. HICKS, AND B. CARRERAS, "The Method of Lines Solution of the Reduced Resistive MHD Equations," ORNL/CSD/TM-133.

26. P. W. GAFFNEY, *in* "Proceedings, Conference on Elliptic PDE's, Santa Fe, New Mexico," Academic Press, New York, in press; P. W. GAFFNEY, "A Survey of Fortran Subroutines Suitable for Solving Stiff Oscillatory Ordinary Differential Equations," ORNL/CSD/TM-134.
27. B. A. CARRERAS, J. A. HOLMES, H. R. HICKS, AND V. E. LYNCH, *Nuclear Fusion* **21** (1981), 511.
28. H. P. FURTH, P. H. RUTHERFORD, AND H. SELBERG, *Phys. Fluids* **16** (1973), 1954.